FDTD Simulation of Hyperbolic Reflection Patterns of Ground Penetrating Radar Images around Subsurface Pipes for Accurate Estimation of Pipe Properties

Rain Man Raja[a,*], Takahiro Yamaguchi[a], Tsukasa Mizutani[a]

[a] *Institute of Industrial Science, the University of Tokyo, 4-6-1, Komaba, Meguro-ku, Tokyo, 153-8505, Japan*

Abstract

The increasing length of the subsurface pipe causes overlapping, accumulating, and sometimes the old pipe layout is not available. Consequently, accidents, damages, time delay and financial losses are occurred during construction of new structures or expanding the roadway or installing of new pipes. Therefore, the depth, diameter, material of the existing pipe as well as the map of the pipe are indispensable to know for appropriate construction planning and development work. Using this algorithm and genetic algorithm optimization, the radius of the field pipe was assessed with 83, 67 and 89% accuracy, the depth was estimated with 95, 95 and 98% accuracy considering the effect of the pipe radius. The effect of the pipe radius should be considered to calculate the pipe depth with higher accuracy. The material of the field pipe was successfully determined using the evaluated relative permittivity of the pipe. A 3D map of the field pipe was developed by applying the tracing algorithm and linear regression to the estimated depth.

Keywords: Grounnd Penetrating Radar (GPR); Multichannel; 3D CNN; Hyperbola Fitting; Pipe Properties; Genetic Algorithm; Tracing Algorithm; 3-D Mapping; Mobile Mapping System (MMS);

1. Introduction

Length of the subsurface utility service pipe is increasing over time. For instance, cumulative length of water supply pipe was about 660 thousand km until 2015 in Japan. [1] Which is responsible for different problems, such as construction planning with no subsurface pipe map causes construction delay and financial loss. [2] Simultaneously, the length of the old subsurface pipe increases and causes various kinds of problems such as leakage of water, washing of soil, caving into the soil, collapse of road surface, etc. [3] Additionally, different utility pipes made of different materials becomes concentrated and cases accidents during excavation of construction works. [2] Another major subsurface pipe is sewage pipe, as of the end of 2020, the total distance of the sewage pipe is about 490 thousand km and about 25 thousand km of pipe is reached its legal lifetime, 50 years. [3] The deterioration and failure of the aged pipes also causes subsurface void or sinkhole and lead to collapse of soil and road surface failure. [4]

Furthermore, different utility pipes are overlapping each other in a city area due to inadequate space and results a complex distribution system. Therefore, maintenance and managing of this huge number of subsurface pipes become very difficult and cumbersome [5] and sometime the unknown position of the subsurface pipes causes mishap and damaged pipes. The surrounding area and economy are impacted by this sort of accidents and damages which is complicated to quantify. [6] For example, over 100 accidents were reported every year by the construction company in Japan. Where only unknown position of subsurface pipe causes about 52% of the accident. [3] The above-mentioned problems are occurred due to lack of information about the depth, diameter, and materials of the subsurface pipe. [7] Additionally, the 2D map of the subsurface pipe does not represent the actual coordinates of the pipe position and makes confusion among the excavation workers. [8] Therefore, depth, diameter and material of the existing subsurface pipe should be estimated accurately, and 3D map with the actual coordinate of the pipe should be produced before any construction works.

2. Literature Review

The subsurface sensing methods like elastic wave, sonic/acoustic, etc. only applicable for non-metallic pipes only. Therefore, a robust method is necessary to detect all types of pipes [9] and a wide range of subsurface utilities both pipe and wire, metallic and plastic pipe can be detected accurately by using the GPR system. [10,11] Consequently, the ground penetrating radar or GPR system become more

* Corresponding author. E-mail: raja_ce@duet.ac.bd

popular for detecting and identifying the subsurface utilities in terms of robustness, time, and accuracy. [12] Additionally, the transmitting and receiving antennas of the GPR system are attached with a vehicle, hence the data acquisition rate is too high, about 80 km of road or surface can be scanned just in one hour. [13,14] Also, the GPR system does not requires any traffic regulation during the data acquisition.

The physics of electromagnetic wave is described by using the Maxwell's equations where the material properties are computed by the constitutive relationships. The finite differences of the Maxwell's equations are calculated in time and space direction using a unique discretization scheme, Yee's algorithm using the Finite Difference Time Domain (FDTD) method. [15] This is the foundation to describe GPR signal quantitively.

Recently, different techniques are using to interpret the GPR data, detecting and estimating the radius of the subsurface pipe such as template matching [16], curve fitting [17], pattern matching [18], neural networks [19], least square approach [20] and theoretical hyperbola. It is difficult to estimate both the diameter and the relative permittivity because there has a clear correlation. [21] Many studies have been done by using only propagation time information or assuming depth of pipe to estimate the relative permittivity or vice versa i.e., those studies avoid the correlation between depth and relative permittivity. [22] The depth of the pipe was estimated from the hyperbolic pattern image assuming or ignoring radius of the pipe in previous work and the estimation deviation for that research was ± 0.1m. [23] The percentage of error was too large for the real field applications.

The Moor Neighborhood algorithm is generally used to detect the boundaries. The average and maximum value for every pixel is estimated using this algorithm. Using the concept of Cellular Automata, the performance of boundary recognition from noisy images are improved. [24,25] The termination condition for this algorithm is to stop after visiting the initial pixel for the second time.

3. Contributions of the research and Methodology

3.1 Contribution of the research

The nonlinear or non-differential problems are solved by the Genetic Algorithm (GA) optimization techniques. The genetic algorithm is an iterative process and searching technique which employed the concept of natural evolution to obtain a rational or the best solution through the natural selection. The main contributions of this research were,

i) Inversely estimate pipes depth, diameter, and material from the shape of reflection pattern and intensity using electromagnetic simulation (FDTD method) and optimization method (Genetic Algorithm)

ii) 3-D mapping of pipes by Moor Neighbourhood tracing and smoothing estimation results

3.2 Methodology

At first the 3D region of the reflected hyperbola was extracted from a large-scale data set using 3D convolution neural network. Then the intensity distribution was extracted along the hyperbola. The radius of the pipe was determined by comparing the field intensity distribution with the intensity distribution of the FDTD simulation. The radius of the field pipe was determined by associating of the peak width of the FDTD simulation database produced by considering different pipe radius. The average of all the radius estimated at each channel was considered as the pipe radius.

Then, a pattern matching algorithm was developed and employed to recognize the shape i.e., hyperbola parameters of the reflected hyperbola. The relationship between depth of the pipe, relative permittivity of the soil with the hyperbola parameters were observed by FDTD simulation models. These relationships display nonlinearity and multi-variability; hence an evaluation function was developed from the fitting criteria of those relationships. After that, the relative permittivity of the field soil and depth of the field pipe were determined inversely by GA optimization using the above evaluation function.

The depth of the pipe and permittivity of the soil were estimated considering the effect of the pipe radius. The accuracy of the depth of the pipe and permittivity of the soil estimation results were improved compared to without considering the effect of pipe radius. The attenuation ratio, the ratio between top of the pipe surface and top of the pavement was used to determine the material of the pipe. A relationship between the attenuation ratio and relative permittivity of the material was established using several FDTD simulation models. Using the measured average attenuation ratio of the field data, relative permittivity of pipe was determined. The pipe material was decided by the considering the standard range of the relative permittivity of different materials.

For the 3D mapping, the Moor neighbourhood tracing algorithm was applied to all the depth point to detect whether they belong to one pipe or not. Then, the layout of the pipe was obtained by applying the linear regression to all the traced depth point and all parameters of the subsurface pipe were shown in the 3D map

4. Measurement system and data

4.1. Measurement system

A vehicle as shown in Fig. 1 with GPR system - a system of antennas, radar transmitter, indicator, data logger and display - was used for the measurement of data. The arrangement of the transmitting and receiving antennas was as shown in Fig. 2. and the system records a position by a GPS and odometer. The antennas are usually installed on the front or the rear of the vehicle and covered with an electromagnetic

Fig. 1. Vehicle With GPR System

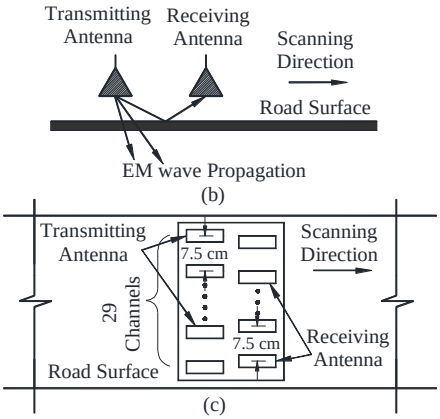

Fig. 2. Antennas arrangement in GPR system [26]

shield to prevent electromagnetic leak out of the system.

A typical measurement system with 29 channels as shown in Fig was used for the survey. The scan pitch was about 0.07m and the height of the antennas was about 0.2m from the road surface. The stepped frequency continuous wave method was applied for the EM wave propagation to detect the subsurface pipe and the operating frequency range was 50 MHz – 3030 MHz with 20 MHz pitch. Additionally, the direct coupling removing filter and a calibration filter of antennas were used during the data acquisition.

4.2. Data

The experimental fields as shown in Fig. 3 and Fig. 4, were prepared with buried pipes and the pipe data was measured by using the above GPR system. This survey was done by expert people and the data was arranged by the scan no., channel no., frequency, real and imaginary parts of Fourier coefficient as a raw text data.

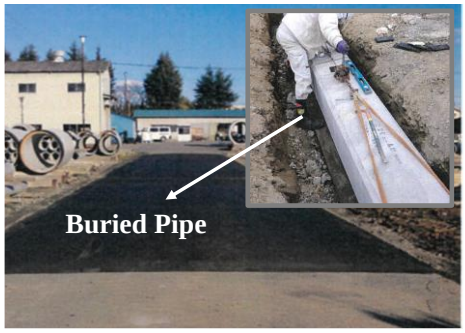

Fig. 3. Experimental Field-1 (Gunma)

Fig. 4. Experimental Field-2 (Hokkaido)

The MATrix LABoratory (MATLAB) is one of the popular applications for the big data analysis. [27] This computational platform has been developed targeting to ease the matrix operation. Therefore, production of training data i.e., conversion of text data to mat data and plotting of the data, analysis of data was done by using MATLAB.

The electromagnetic FDTD simulations were done by using gprMax, an open source, python-based program for the simulation of electromagnetic wave for GPR system. [28] Since the volume of data is huge, hence GPU system was used for the FDTD simulation, generating database, developing, and validating the algorithms. Additionally, a denoising filter was applied to the experimental field data to obtain a strong intensity distribution and reflection pattern. [29] Among the several image filter techniques, the subtract mean or mean data filter technique as shown in Fig. 5, which reduce the variation of pixel intensities of the image, is easy and intuitive to apply for the image enhancement. Therefore, the subtraction of the mean image filter was deployed for the denoising of the experimental data in this research.

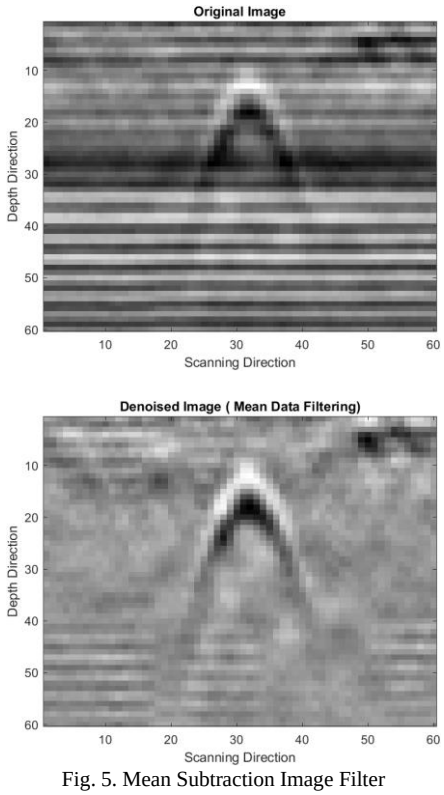

Fig. 5. Mean Subtraction Image Filter

5. Simulation model

Reflection and refraction are occurred at each boundary of the multilayer layer subsurface during the EM wave propagation and the propagation does not follow the same path due to the position of transmitting and receiving antennas. Which causes a multivariate and nonlinear relation, and which cannot be solved explicitly. Electromagnetic simulation by FDTD method was conducted for multilayer condition to overcome this problem and this FDTD simulation database was used to match with the measured data. The multilayer models were as shown in Fig. 7 was used for the simulations.

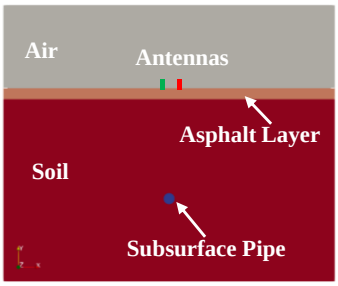

Fig. 7. Simulation Model

Several thousand of simulations were performed during the research work and the calculation time for each simulation model depends on the size of discretization. Additionally, smaller discretization is essential for the higher level of accuracy and 1mm discretization was used for the simulation in this research. High configured computer with higher GPU is required for the faster EM simulation and the PCs with the following GPU, NVIDIA GeForce RTX 2080 and NVIDIA GeForce RTX 1080Ti were used simultaneously for the several simulations. The gprMax application was used for the EM simulation and the EM wave propagation for the simulation at different time were shown in the following Fig. 8.

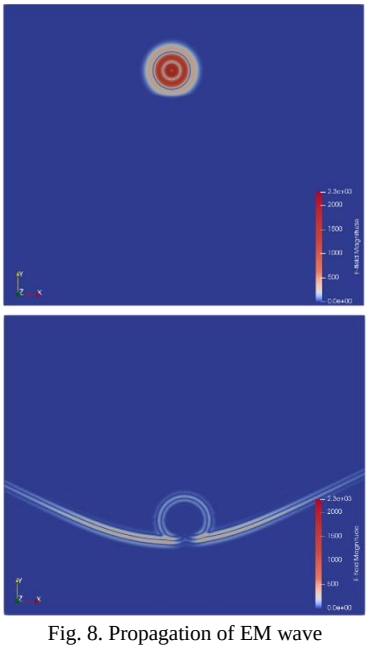

Fig. 8. Propagation of EM wave

6. Algorithms and Validations

6.1. Basic algorithms

The developed algorithm for the estimation of the properties of the subsurface pipe consist of some steps. The flow diagram of the developed algorithm is as following,

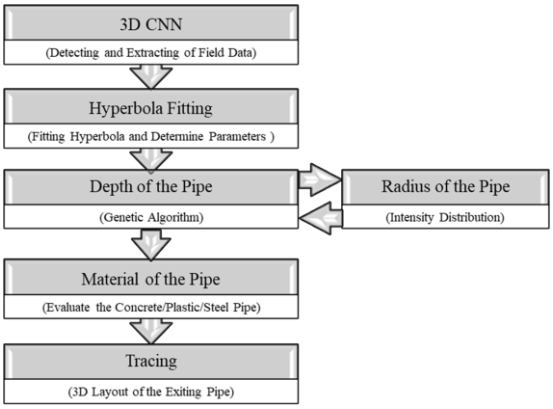

Fig. 9. Flow Diagram of Algorithm

6.1.1 3D CNN

The 3D Convolution Neural Network developed by Dr. Takahiro Yamaguchi, Mizutani Lab, the University of Tokyo, was used on the experimental field data to detect the 3D region of the hyperbolic shape. This 3D CNN, deep learning method localize the 3D reflection pattern as shown in Fig. 10, which reduce the calculation time. For that, the target region was extracted by using 3D-CNN from a large-scale data. About 29-2D data set were obtained for the 29 channels from the extracted 3D region.

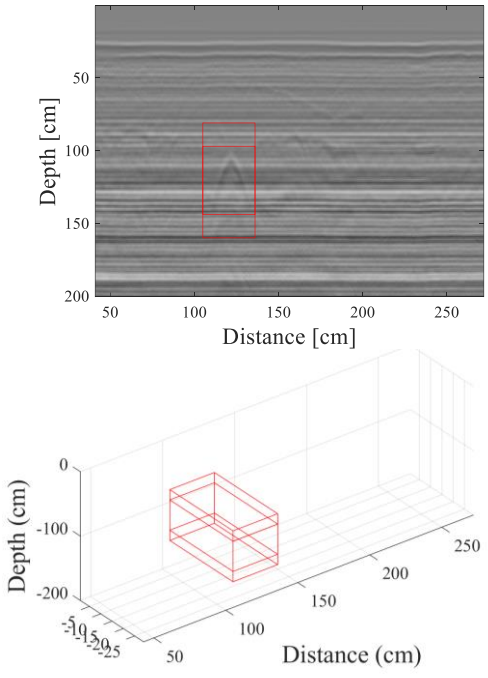

Fig. 10. Application of 3D CNN

6.1.2. Hyperbola fitting

Higher dimensional fitting equation including the pipe radius does not represent hyperbola and causes an unstable solution for the parameter estimation. Therefore, the radius of the pipe was estimated individually. Then, a pattern recognition algorithm was developed based on this simple mathematical equation,

$$\frac{x^2}{a^2} - \frac{y^2}{b^2} = 1 \quad \ldots\ldots\ldots\ldots\ldots\ldots \text{(i)}$$

where a and b are the hyperbola parameters. This hyperbola parameters were employed for the development of the algorithm. A pattern recognition approach was used to know the parameters of the reflected hyperbola. About 1000 binary data set, using the range of the hyperbola parameter b, was produced and 2D cross correlation with the field data was observed as shown in Fig. 11.

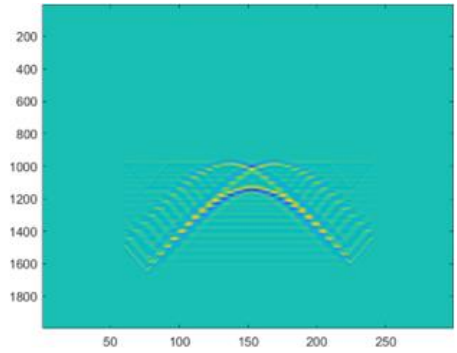

Fig. 11. Cross Correlation

This correlation function returns a cross correlation value for each binary hyperbola and the reflected hyperbolic shape. The maximum correlated value as shown in Fig. 12 represents the best fitted hyperbola.

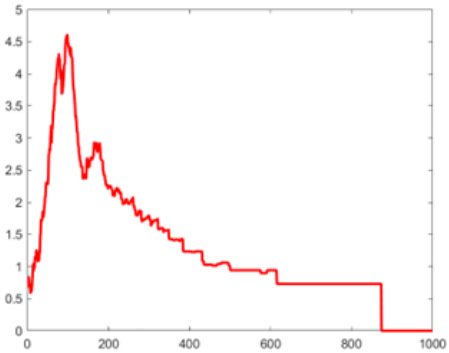

Fig. 12. Cross correlations values for 1000 binary dataset

6.1.3. Radius of the pipe

The intensity distribution of FDTD simulation model was observed after up sampling the data in the depth direction and applying the mean subtraction. The radius of in the real field varies from 2.5 cm to 40 cm. The pipe sizes considered in the FDTD simulation model were 0.5, 1, 5, 10, 15, 20, 25, 30, 35, 40, 45 and 50 cm. The peak width between the points of intensity distribution of the experimental field data were compared with the peak width of the intensity distribution of the simulation data as shown in Fig. 13.

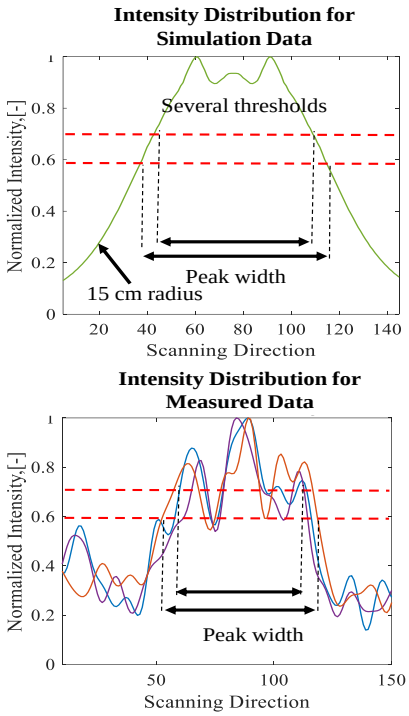

Fig. 13. Pipe radius calculation from intensity distribution

All the radius for 29 channels calculated from the intensity distribution by comparing the peak width of field intensity distribution at different normalized value were noted. The average of all recorded data was considered as the radius of the field pipe.

6.1.4. Depth of the pipe

The relationships of hyperbola parameters with depth of the pipe and relative permittivity of soil have been observed using the FDTD simulation database. Where a particular pipe depth shows a nonlinear relationship between hyperbola parameter b and relative permittivity of soil and this relationship varies with the different pipe depths. Therefore, a multivariate, nonlinear relationship has been developed from the FDTD simulation database. An evaluation function was developed based on the fitting relationship as shown in Fig. 14 of this FDTD simulation database.

The field pipe depth, d and relative permittivity of soil, ε were inversely estimated from the hyperbola parameters, a and b. The genetic algorithm (GA) optimization was employed to evaluate the depth of pipe and relative permittivity of the field soil by optimization process. The depth estimation was improved by considering the effect of the pipe radius than without considering pipe radius. The equation (ii) represents the evaluation function for the following fitting relationship shown in Fig. 14.

$$Eval = (Y - (-3.4 + 22.7 \times x_1 + 0.4 \times x_2 - 5.9 \times (x_1)^2 + 0.3 \times x_1 \times x_2 - 0.0 \times (x_2)^2))^2 + (Z - (-23.9 + 75.9 \times x_1 + 2.0 \times x_2 + 2.7 \times (x_1)^2 + 14.2 \times x_1 \times x_2 - 0.3 \times (x_2)^2))^2 \ldots \text{(ii)}$$

Where, Y is the hyperbola parameter b, Z is the hyperbola parameter a, x_1 is the depth of the pipe, x_2 is the relative permittivity of soil.

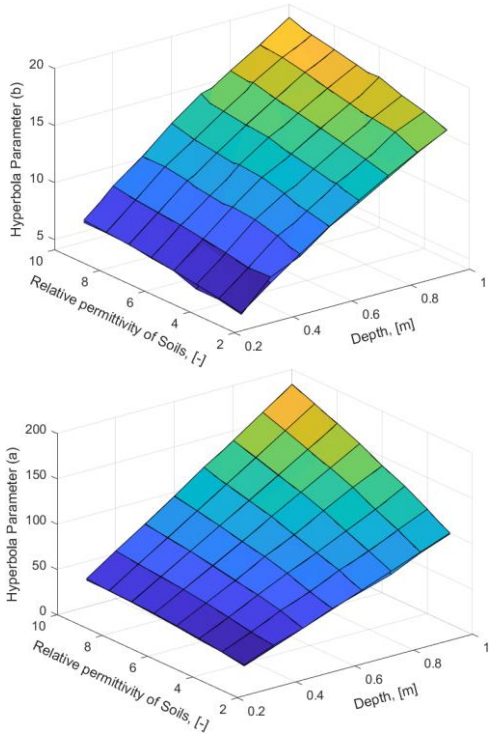

Fig. 14. Fitting relationship between the hyperbola parameters and relative permittivity of soil and depth of the pipe

6.1.5. Material of the pipe

The most common materials of the pipe using for water supply, sewage system and others are plastic, concrete, and steel. [28][29] The material of the pipe was estimated inversely by the attenuation ratio using the known depth and radius. The attenuation ratio is defined as the ratio of the intensity of the pipe reflection and intensity of the asphalt surface. Then several FDTD simulation models were prepared and executed by using different permittivity of pipe material and the attenuation ratio was recorded for each simulation case. Finally, a relationship between the relative permittivity of the pipe and the attenuation ratio was prepared.

Then, the attenuation ratio of the experimental field data was estimated for all the 29 channels. The average of the attenuation ratio was taken and using the above relationship the permittivity of the experimental field pipe was determined as shown in Fig. 15.

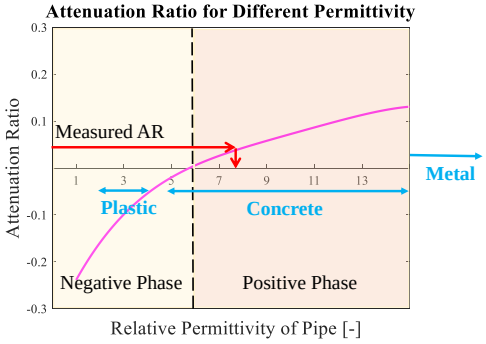

Fig. 15. Pipe material determination

When the permittivity of the pipe material was found between the range 2 to 4 then the pipe was defined as plastic pipe. [30] The pipe was defined as concrete when the permittivity of the pipe material lies between 5 to 20. For the infinitely large permittivity of the material represents the steel pipe. [31]

6.1.6. Tracing and 3D Mapping

The tracing of the pipe was applied to detect all the estimated depth point belongs to one point or not. The layout of the pipe in the longitudinal direction was obtained by employing linear regression to all the estimated depth. Since Moor Neighborhood tracing algorithm is a popular and easy to detect the trace point hence this algorithm was used for the tracing of the subsurface pipe.

According to this algorithm, the angle of the candidate points was calculated in clockwise direction from the initial points and candidate point with smaller angle was selected as the next trace point. Similar approach was applied for the other points and all the trace points were determined. This procedure ends when the tracing algorithm return to the initial point. The following Fig. 16. shows the used tracing algorithm of the pipe in 3D region. Then, applying the linear regression to all the traced depth point, the layout of the pipe was obtained, and all parameters of the subsurface pipe were shown in the 3D map.

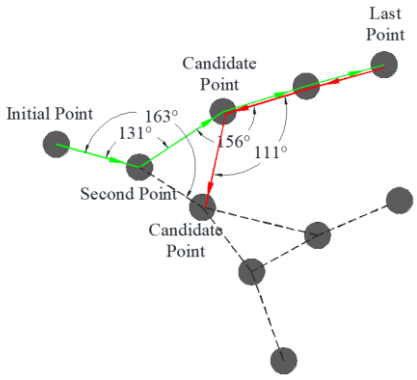

Fig. 16. Moor Neighbourhood tracing algorithm

6.2. Validation of Algorithm

The developed algorithm was employed to detect the properties of pipe for different experimental fields data and varying the bituminous pavement thickness. The target pipes of the different experimental fields are as shown in Fig. 17 and Fig. 18. The estimated pipe properties, radius, depth, and material for different experimental field have been discussed in result and discussion section.

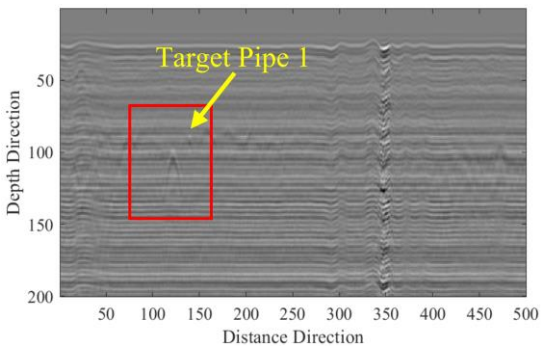

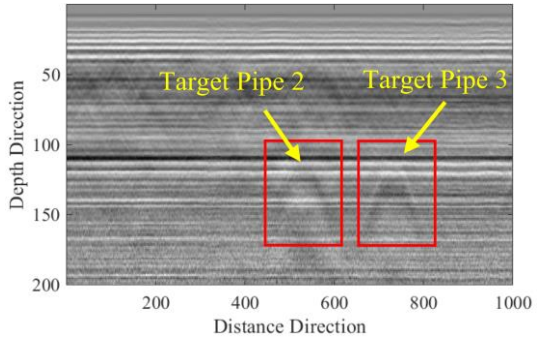

Fig. 18. Target Pipes from Experimental Field-2

7. Results and Discussion

7.1. Radius of the field pipe

After comparing the intensity distribution of the experimental field data with the intensity distribution of the simulation database, the radius of the pipes was obtained as the following Table 1. The accuracy of the estimated mean radius for the Target pipe 1, Target pipe 2 and Target pipe 3 were 83%, 67%, and 89% respectively.

Table 1: Estimated pipe radius for different target

Target	Estimated Radius, [cm]	True Radius, [cm]
Pipe 1	17.5	15
Pipe 2	13.3	10
Pipe 3	11.1	10

The estimation result of the pipe radius can be improved if there is more smooth intensity distribution along the hyperbola of the field data. For Target pipe 2, the accuracy of the radius estimation was lower than the other because of the image was not improved enough even applying the filter. Although, the field data have lots of noises and disturbance in the intensity distribution along the hyperbola, this level of accuracy is applicable in the field survey.

7.2. Depth of the field pipe

The depth of the field pipe and relative permittivity of the filed soil optimized inversely by the genetic algorithm (GA) using the evaluation function with considering the effect of the pipe radius. The estimated depth of the different target pipes at different channels were as the following Fig. 19, Fig. 20, and Fig. 21.

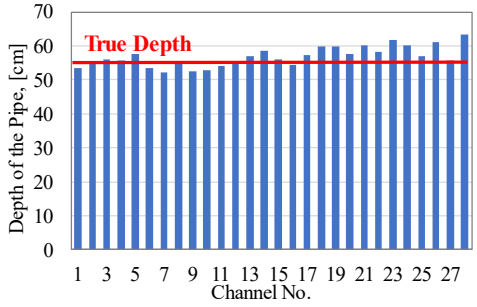

Fig. 19. Depth at different channels of Target Pipe 1

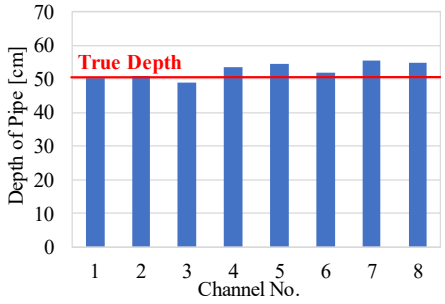

Fig. 20. Depth at different channels of Target Pipe 3

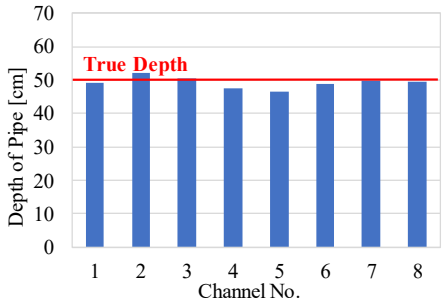

Fig. 21. Depth at different channels of Target Pipe 3

The depths of the Target pipe 1, Target pipe 2 and Target pipe 3 were determined with 4.9%, 5.0% and 1.6% error respectively. This accuracy is higher than the other research works which were done without considering the effect of the pipe radius. The depths of the pipe for different experimental fields are as following Table 2.

Table 2: Estimated pipe depth for different target

Target	Estimated Depth, [cm]	True Depth, [cm]
Pipe 1	57.7	55
Pipe 2	52.5	50
Pipe 3	49.2	50

The field pipe depth without considering the effect of the pipe radius for different target pipe were 45.3 cm, 48.4 cm, and 44.8 cm respectively. These results illustrate large error than the considering the effect of pipe radius as like the previous research works. Therefore, the pipe radius effect should be considered for the higher accuracy in the depth estimation of the subsurface pipe.

7.3. Material of the pipe

The attenuation ratio of the Target pipe 1, Target pipe 2 and Target pipe 3 were determined 0.0463, -0.0712 and 0.015 respectively. The relative permittivity of the different pipes was estimated from the relationship of attenuation ratio and relative permittivity as shown in Fig. The material of the pipe was estimated inversely from this relative permittivity. Usually, the relative permittivity of steel pipe is infinity large compared to other pipes. On the other hand, the permittivity of plastic is smaller than the permittivity of soil and the permittivity of concrete pipes ranges between 5 to 20. The pipe materials for

the different Target pipes were shown in the following Table 3.

Table 3: Calculated pipe materials for different target

Target	Relative Permittivity	Evaluated Pipe Material	True Pipe Material
Pipe 1	7.5	Concrete	Concrete
Pipe 2	2.7	Plastic	Plastic
Pipe 3	5.5	Concrete	Concrete

7.4. 3D mapping of pipe

The accurate depth of the different field pipes was determined at each channel by the developed algorithm and genetic algorithm optimization. The Moor Neighborhood algorithms was applied to trace the depth points which were belong to one pipe. After getting the traced points, the linear regression was applied along the pipe direction to obtain layout of the pipe. The following Fig. 22, Fig. 23, and Fig. 24 are showing the traced points and the 3D layout of the different target pipes.

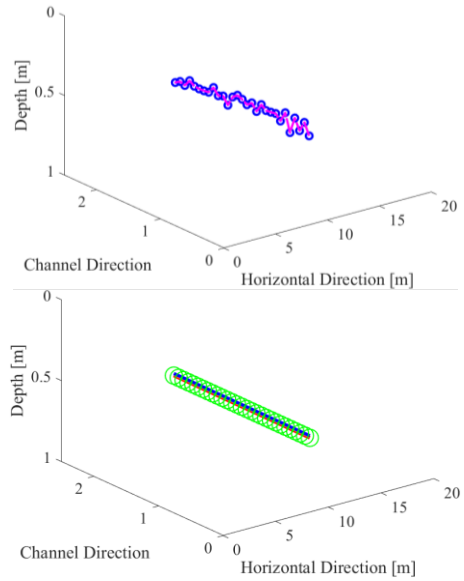

Fig. 22. 3D mapping of Target pipe 1

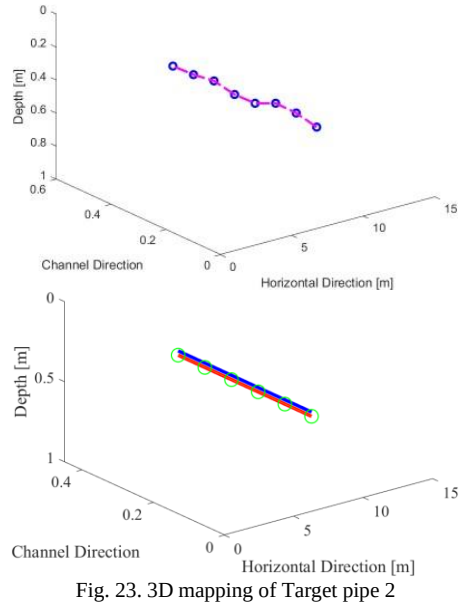

Fig. 23. 3D mapping of Target pipe 2

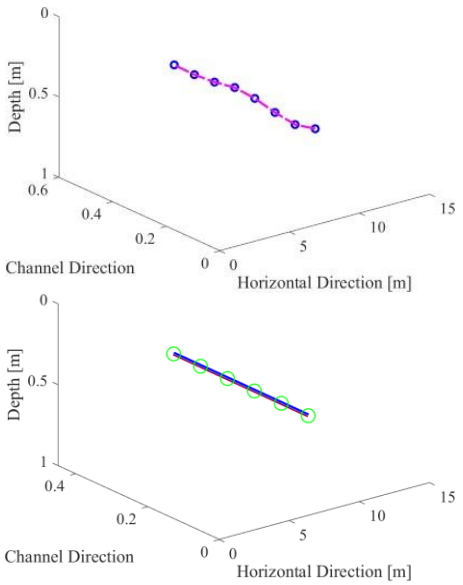

Fig. 24. 3D mapping of Target pipe 3

7.5. Bituminous pavement thickness

The thickness of the bituminous layer was considered about 10 cm for all the FDTD simulation models. There is minor effect on the estimation of the depth and diameter of the pipe for a small variation of the pavement thickness. For instance, decreasing the pipe thickness to 5 cm increase the depth of the pipe 1 to 2 cm. Where, the developed algorithm shows large error of properties estimation for the large variation of pavement thickness compared to the simulation model thickness.

8. Conclusions

3D CNN was applied to extract the hyperbolic region from a large-scale data and a pattern matching algorithm was developed to detect the hyperbolic shape of reflection. Since, the relationship of hyperbola parameters with the depth of the pipe and the relative permittivity of soil was a nonlinear, multivariate hence the Genetic Algorithm optimization was applied to optimize the field pipe depth and the relative permittivity of the soil. For that an evaluation function was developed from the relationships of hyperbola parameters, depth of the pipe and the relative permittivity of soil using several FDTD simulation data.

The parameters were estimated by genetic algorithm. The radius of the pipe was estimated from the intensity distribution along the hyperbola of the filed data. All the validation cases, the pipe radius was estimated with an acceptable accuracy and this limit of accuracy can be applicable for the field investigation. The depth of the pipe was estimated successfully, and for all the validation cases, the accuracy of the estimation was 95% or more. This accuracy was achieved by considering the effect of the pipe radius. Therefore, effect of the pipe radius is not negligible and should be considered for the accurate estimation of the pipe depth. The relative permittivity of the pipe

was determined from the relationship of attenuation ration and permittivity of the material developed by FDTD simulation database. The material of the pipe was determined successfully for all the field pipes.

Moor Neighbourhood tracing algorithm was applied to trace the depth location in 3D region for all channels along the pipe direction and the 3D map of the pipe was developed. After applying the linear regression to all the pipe depth, the 3D map of the pipe with the actual pipe depth was plotted successfully. This type of 3D plot can be employed in the real field for smooth construction works by avoiding damage of pipe, construction delay and financial loss.

Acknowledgement

The author is obliged to Professor Dr. Riki Honda, UTokyo for his valuable instructions and observations throughout the research work. The authors want to express gratitude to the related engineers of C. E. Management Integrated Laboratory Co., Ltd., Nagano prefecture, Japan, Fujimura Crest Co., Ltd., Niigata prefecture, Japan for their support by providing the experimental data for this research.

References

[1] J. W. W. Association, “Water Supply in Japan 2017,” 2017. [Online]. Available: http://www.jwwa.or.jp/jigyou/kaigai_file/2017WaterSupplyInJapan.pdf

[2] A. Sharafat, M. S. Khan, K. Latif, W. A. Tanoli, W. Park, and J. Seo, “BIM - GIS - Based Integrated Framework for Underground Utility Management System for Earthwork Operations,” *Appl. Sci.*, vol. 11, no. 12, p. 5721, Jun. 2021, doi: 10.3390/app11125721.

[3] “Sewerage: Maintenance and Management of Sewerage - Ministry of Land, Infrastructure, Transport and Tourism.” https://www.mlit.go.jp/mizukokudo/sewerage/crd_sewerage_tk_000135.html (accessed Sep. 05, 2022).

[4] J. P. Davies, B. A. Clarke, J. T. Whiter, and R. J. Cunningham, “Factors influencing the structural deterioration and collapse of rigid sewer pipes,” *Urban Water*, vol. 3, no. 1, pp. 73–89, 2001, doi: https://doi.org/10.1016/S1462-0758(01)00017-6.

[5] M. Wang, Y. Deng, J. Won, and J. C. P. Cheng, “An integrated underground utility management and decision support based on BIM and GIS,” *Autom. Constr.*, vol. 107, p. 102931, 2019, doi: https://doi.org/10.1016/j.autcon.2019.102931.

[6] N. Metje, B. Ahmad, and S. M. Crossland, “Causes, impacts and costs of strikes on buried utility assets,” *Proc. Inst. Civ. Eng. Munic. Eng.*, vol. 168, no. 3, pp. 165–174, 2015, doi: 10.1680/jmuen.14.00035.

[7] B. T. Kolera and L. E. Bernold, “Intelligent Utility Locating Tool for Excavators,” *J. Constr. Eng. Manag.*, vol. 132, no. 9, pp. 919–927, Sep. 2006, doi: 10.1061/(ASCE)0733-9364(2006)132:9(919).

[8] J. Guerrero, S. Zlatanova, and M. Meijers, “3D visualisation of underground pipelines: Best strategy for 3D scene creation,” *ISPRS Ann. Photogramm. Remote Sens. Spat. Inf. Sci.*, vol. 2, no. 2W1, pp. 139–145, 2013, doi: 10.5194/isprsannals-II-2-W1-139-2013.

[9] W. Al-Nuaimy, Y. Huang, M. Nakhkash, M. T. C. Fang, V. T. Nguyen, and A. Eriksen, “Automatic detection of buried utilities and solid objects with GPR using neural networks and pattern recognition,” *J. Appl. Geophys.*, vol. 43, no. 2, pp. 157–165, 2000, doi: https://doi.org/10.1016/S0926-9851(99)00055-5.

[10] H. M. Jol, *Ground Penetrating Radar Theory and Applications*. Elsevier Science, 2008.

[11] W. A. Wahab, J. Jaafar, I. M. Yassin, and M. R. Ibrahim, “Interpretation of Ground Penetrating Radar (GPR) image for detecting and estimating buried pipes and cables,” *Proc. - 2013 IEEE Int. Conf. Control Syst. Comput. Eng. ICCSCE 2013*, vol. 0, pp. 361–364, 2013, doi: 10.1109/ICCSCE.2013.6719990.

[12] W. Muller, “A network-level road investigation trial using Australian-made traffic-speed 3D ground penetrating radar (GPR) technology,” in *25th ARRB Conference*, 2012, pp. 1–18.

[13]A. Benedetto, F. Tosti, L. Bianchini Ciampoli, and F. D’Amico, “An overview of ground-penetrating radar signal processing techniques for road inspections,” *Signal Processing*, vol. 132, pp. 201–209, 2017, doi: 10.1016/j.sigpro.2016.05.016.

[14] W. Li, M. Burrow, N. Metje, and G. Ghataora, “Automatic Road Survey by Using Vehicle Mounted Laser for Road Asset Management,” *IEEE Access*, vol. 8, pp. 94643–94653, 2020, doi: 10.1109/ACCESS.2020.2994470.

[15] J.-M. Jin, *Theory and computation of electromagnetic fields*. John Wiley & Sons, 2011.

[16] N. Rachmana, Hendrawan, Sugihartono, and A. B. Suksmono, “Interpretation target pattern of a buried basic object on Surface Ground Penetrating Radar system,” in *2009 International Conference on Electrical Engineering and Informatics*, 2009, vol. 02, pp. 553–558. doi: 10.1109/ICEEI.2009.5254752.

[17] S. W. Jaw, M. Hashim, and M. Marghany, “New approach for extraction of subsurface cylindrical pipe diameter and material type from ground penetrating radar image,” in *31st Asian Conference on Remote Sensing 2010, ACRS 2010*, Jan. 2010, vol. 2, pp. 1187–1193.

[18] E. Pasolli, F. Melgani, and M. Donelli, “Automatic Analysis of GPR Images: A Pattern-Recognition Approach,” *IEEE Trans. Geosci. Remote Sens.*, vol. 47, no. 7, pp. 2206–2217, 2009, doi: 10.1109/TGRS.2009.2012701.

[19] S. Shihab, W. Al-Nuaimy, and A. Eriksen, “Image processing and neural network techniques for automatic detection and interpretation of ground penetrating radar data,” *Recent Adv. Circuits, Syst. Signal Process.*, pp. 360–363, 2002, doi: 0018–926X/99$10.00.

[20] A. Dolgiy, A. Dolgiy, and V. Zolotarev, “Optimal radius estimation for subsurface pipes detected by ground penetrating radar,” in *Proceedings 11th International Conference on Ground Penetrating Radar, Columbus, Ohio, USA*, 2006, vol. 4.

[21] N. Muniappan, A. V Hebsur, E. P. Rao, and G. Venkatachalam, “Radius estimation of buried cylindrical objects using GPR - A case study,” in *2012 14th International Conference on Ground Penetrating Radar (GPR)*, Jun. 2012, pp. 789–794. doi: 10.1109/ICGPR.2012.6254969.

[22] H. Hayakawa and A. Kawanaka, “Radar imaging of underground pipes by automated estimation of velocity distribution versus depth,” *J. Appl. Geophys.*, vol. 40, no. 1–3, pp. 37–48, 1998, doi: 10.1016/S0926-9851(98)00028-7.

[23] S. W. Jaw and M. Hashim, “Locational accuracy of underground utility mapping using ground penetrating radar,” *Tunn. Undergr. Sp. Technol.*, vol. 35, pp. 20–29, Apr. 2013, doi: 10.1016/j.tust.2012.11.007.

[24] S. Uguz, H. Akin, I. Siap, and U. Sahin, “On the irreversibility of Moore cellular automata over the ternary field and image application,” *Appl. Math. Model.*, vol. 40, no. 17, pp. 8017–8032, 2016, doi: https://doi.org/10.1016/j.apm.2016.04.027.

[25] P. Sharma, M. Diwakar, and N. Lal, “Edge Detection using Moore Neighborhood,” *Int. J. Comput. Appl.*, vol. 61, no. 3, pp. 26–30, 2013, doi: 10.5120/9910-4506.

[26] T. Yamaguchi, T. Mizutani, and T. Nagayama, “Mapping Subsurface Utility Pipes by 3-D Convolutional Neural Network and Kirchhoff Migration Using GPR Images,” *IEEE Trans. Geosci. Remote Sens.*, vol. 59, no. 8, pp. 6525–6536, 2021, doi: 10.1109/TGRS.2020.3030079.

[27] S. D. Bradley, “Matlab,” in *The International Encyclopedia of Communication Research Methods*, Wiley, 2017, pp. 1–3. doi: 10.1002/9781118901731.iecrm0136.

[28] C. Warren, A. Giannopoulos, and I. Giannakis, “gprMax: Open source software to simulate electromagnetic wave propagation for Ground Penetrating Radar,” *Comput. Phys. Commun.*, vol.

209, pp. 163–170, 2016, doi: https://doi.org/10.1016/j.cpc.2016.08.020.

[29] M. Szymczyk and P. Szymczyk, “Preprocessing of GPR data,” *Ipc*, vol. 18, no. 2–3, pp. 83–90, 2013, doi: 10.2478/v10248-012-0082-3.

[30] N. Reyes, F. Casado, V. Tapia, C. Jarufe, R. Finger, and L. Bronfman, “Complex Dielectric Permittivity of Engineering and 3D-Printing Polymers at Q-Band,” *J. Infrared, Millimeter, Terahertz Waves*, vol. 39, no. 11, pp. 1140–1147, 2018, doi: 10.1007/s10762-018-0528-9.

[31] F. Luis and G. Moncayo, *Ground-Penetrating Radar for Archaeology*. Published by AltaMira Press, 2013.